A novel diagnostic for dust particle size in a low-pressure nanodusty plasma based on the decay of the electron density released by laser-induced photodetachment

A novel diagnostic for dust particle size in a low-pressure nanodusty plasma based on the decay of the electron density released by laser-induced photodetachment

T. J. M. Donders ✉ ⓘ ; T. J. A. Staps ⓘ ; J. Beckers ⓘ

Check for updates

View Online   Export Citation   CrossMark

Articles You May Be Interested In

Spatiotemporal evolution of a self-excited dust density wave in a nanodusty plasma under strong Havnes effect

Physics of Plasmas (December 2021)

Optical emission spectroscopy of microwave-plasmas at atmospheric pressure applied to the growth of organosilicon and organotitanium nanopowders

Journal of Applied Physics (March 2014)

In-situ analysis of optically thick nanoparticle clouds

Appl. Phys. Lett. (April 2017)

A novel diagnostic for dust particle size in a low-pressure nanodusty plasma based on the decay of the electron density released by laser-induced photodetachment

View Online   Export Citation   CrossMark

T. J. M. Donders,[a] (iD) T. J. A. Staps, (iD) and J. Beckers (iD)

AFFILIATIONS

Department of Applied Physics, Eindhoven University of Technology, PO Box 513, 5600MB Eindhoven, The Netherlands

[a]Author to whom correspondence should be addressed: t.j.m.donders@tue.nl

ABSTRACT

One of the key parameters in low-pressure nanodusty plasmas is the dust particle size. In this work, we introduce a new method for the determination of the dust particle size in a nanodusty plasma, created in a mixture of argon and hexamethyldisiloxane. To this end, an ultraviolet ($\lambda = 266$ nm) pulsed laser was used to release plasma-collected electrons from the nanoparticles. Subsequently, the response of the free electron density of the plasma was measured using microwave cavity resonance spectroscopy. Using a stochastic model for particle charging using orbital-motion limited (OML) theory, the predicted charging timescale can be directly compared to the experimentally measured decay timescale of the photo-released electron density. Good agreement was found between the experimentally predicted dust particle size and *ex situ* scanning electron microscopy (SEM) measurements. Furthermore, the sensitivity of the OML model to its input parameters was assessed. Finally, reversing the method can yield an estimate for the positive ion density based on the dust particle size from SEM.

I. INTRODUCTION

A dusty plasma constitutes a partially ionized gaseous medium containing charged solid dust particles with a typical size ranging from several nanometers to micrometers.[1,2] Examples of dusty plasmas can be found both in the field of astrophysics[3] and in industrial applications.[4] Astrophysical phenomena, such as accretion disks[5] or planetary rings,[6,7] show large-scale dust structures, both in the sense of dust particle size and in terms of spatial dimensions. In industry, such as in the field of photolithography,[8] dust particles are often seen as a form of contamination.[9,10] The current research is, therefore, performed on methods to control the contamination in low-pressure plasma applications.[11–13]

In order to understand the behavior of dust particles in these applications, dusty plasmas are investigated in laboratory environments. Since dust particles in a plasma behave as electrostatically floating probes,[2] they will become electrically charged by collecting free electrons and ions from the plasma. Due to the fact that electrons are much lighter and therefore more mobile compared to ions, the equilibrium charge of a dust particle will generally be negative in the plasma

bulk region. Under certain conditions, the dust particles and the plasma environment can be strongly coupled, which will give rise to phenomena such as dust crystallization,[14–16] phase transitions,[17] self-excited dust density waves,[18–20] and chain formation.[21]

All of these effects are fundamentally driven by the dust particle charge, which makes it one of the key parameters in dusty plasma physics. The charge of a dust particle in a plasma is mainly determined by the (local) densities and temperatures of the plasma species and by the size of the dust particle. The charge of microparticles has previously been measured using particle resonance methods[22,23] or by means of applying external electric fields.[11,12] In the case of nanodusty plasmas, the total charge density has previously been measured using laser-induced photodetachment.[24]

Apart from the particle charge, the particle size also plays a major role in dusty plasma physics. Especially in the case of nanodusty plasmas, where the dust particles are chemically grown *in situ* instead of being externally injected, the evolving dust particle size has consequences for the general behavior of the plasma. A typical nanodusty plasma is created in a gas mixture of a noble background gas and a

reactive precursor gas. Typical examples of precursor gases used for dusty plasma research and in applications are acetylene (C_2H_2),[25–28] methane (CH_4),[29,30] silane (SiH_4),[31] and organosilicon precursors, such as hexamethyldisiloxane [HMDSO ((CH_3)$_3$–Si–O–Si–(CH_3)$_3$)][32–35] that was used in this work. HMDSO can be found in industrial applications, such as superhydrophobic coatings,[36] and it is seen as a cosmic dust analogue in the field of astrophysics.[37] Furthermore, HMDSO is favorable from the viewpoint of its experimental convenience, as it is liquid under standard pressure and room temperature.

In such plasmas, solid particles are generated by polymerization reactions of precursor species. Generally, dust growth in reactive plasmas happens in three distinct phases.[4] During the nucleation phase, the first negative ions are formed by electron attachment reactions with free electrons from the plasma, which sets the course for polymerization with more precursor molecules into small clusters. As soon as the cluster density is sufficiently high, the coagulation phase starts in which clusters suddenly coalesce into particles with a size of several tens of nanometers. At the end of this phase, all particles have typically obtained a permanently negative charge, which inhibits further coagulation. As a result, the particles will enter the accretion phase, during which they grow by the collection of positive ions and radicals from the plasma. For nanoparticles, gravity is usually neglected, such that the force balance on such particles is governed by the (confining) electrostatic force and the (oppositely directed) ion drag force. As the particles grow further in size, the magnitude of the latter force outweighs the former, which leads to particles eventually leaving the discharge. Typically, the particles then reach sizes of a few hundreds of nanometers.

In the past, nanodusty plasmas have been investigated both numerically and experimentally. In the numerical field, reaction schemes for complex plasma chemistries have been constructed,[38–40] from which sophisticated numerical models for the formation and subsequent growth of nanoparticles out of plasma species have been built.[41–46] Furthermore, experimental methods for measuring the dust particle size, such as Mie ellipsometry,[47–55] light extinction spectroscopy (LES),[56,57] and time-resolved laser-induced incandescence (TIRE-LII),[58–61] have been developed. More recently, we presented a method for determining the dust particle size and the dust density based on the combination of laser light extinction and electron density measurements.[62]

In this work, we present a novel method for determining the dust particle size, based on the detachment of electrons bound to the dust particles upon irradiation with pulsed ultraviolet (UV) laser light. We have experimentally measured the additional free electron density in the plasma after the laser pulse, from which we show that the dust particle size can be determined from the re-charging timescale. Using the combination of experiments and modeling, we are able to determine the dust particle size starting from several tens of nanometers while being minimally intrusive.

This work is structured as follows: Sec. II establishes the theoretical framework by providing a stochastic model for determining the dust (re-)charging timescale of a dust particle after a photodetachment incident. In Sec. III, the experimental setup is discussed and the experimental procedure is explained. Subsequently, Sec. IV shows the results of the measurements and uses the developed model to determine the dust particle size. Eventually, Sec. V summarizes the work and provides the conclusions.

II. A STOCHASTIC MODEL FOR DETERMINING THE DUST (RE-)CHARGING TIMESCALE UPON ELECTRON DETACHMENT BY UV RADIATION

In this section, a model for the (re)charging of a dust particle in a plasma environment will be provided. The model is an adapted implementation of the work of Cui and Goree.[63] In this work, the basics of the model are briefly summarized, and the emphasis is on the modifications necessary to make this model suitable for a nanodusty plasma.

The widely accepted Orbital Motion Limited (OML) theory[64] lies at the basis of the model. It describes the charging of dust particles in the bulk of a plasma, which is governed by the collection of electrons and positive ions. Since the electron mobility is much higher than the ion mobility, dust particles tend to charge negatively. In this case, plasma electrons are subjected to a repulsive surface potential, while ions will be attracted to the (now negatively charged) dust particle. For electrons (I_e) and positive ions (I_{i+}), the OML collection currents toward a plasma-immersed particle with radius a, therefore, can be stated as

$$I_e = -en_e\pi a^2 \sqrt{\frac{8k_B T_e}{\pi m_e}} \exp\left(-\frac{-e\Phi_d}{k_B T_e}\right), \tag{1}$$

$$I_{i+} = en_{i+}\pi a^2 \sqrt{\frac{8k_B T_{i+}}{\pi m_{i+}}}\left(1 - \frac{e\Phi_d}{k_B T_{i+}}\right). \tag{2}$$

In these equations, e is the elementary charge, and k_B is the Boltzmann constant. Furthermore, $n_{e,i+}$, $T_{e,i+}$, and $m_{e,i+}$ are the densities, temperatures, and masses of electrons and positive ions, respectively. Finally, Φ_d is the surface potential of the dust particle. The latter can be used to calculate the dust particle charge Q_d using the capacitance of a sphere C_{sphere},

$$Q_d = C_{sphere}\Phi_d = 4\pi\varepsilon_0 a\left(1 + \frac{a}{\lambda_{De}}\right)\Phi_d \approx 4\pi\varepsilon_0 a\Phi_d. \tag{3}$$

In this equation, ε_0 is the vacuum permittivity, and λ_{De} is the electron Debye length. In this equation, it is assumed that the particle is spherical and it can be verified that the typical particle size is much smaller than the electron Debye length ($a/\lambda_{De} \ll 1$). Next, the transient behavior of the (re-)charging of a dust particle is governed by the following differential equation:

$$\frac{dQ_d}{dt} = I_e + I_{i+}. \tag{4}$$

This equation could be solved by direct numerical integration, but a stochastic approach better captures the physics of the charging process, as it takes into account individual electrons and ions arriving at the particle surface. This stochastic model is schematically depicted in Fig. 1 and works as follows:

- As an input, values for the dust particle size and the electron and positive ion densities $n_{e,i+}$ and temperatures $T_{e,i+}$ need to be provided. Then, a lookup table for the electron and positive ion particle currents ($p_{e,i+} = I_{e,i+}/e$) toward the particle as a function of particle charge will be generated using Eqs. (1)–(3).
- The actual simulation begins with choosing a dust particle size and setting the starting condition for the dust particle charge.
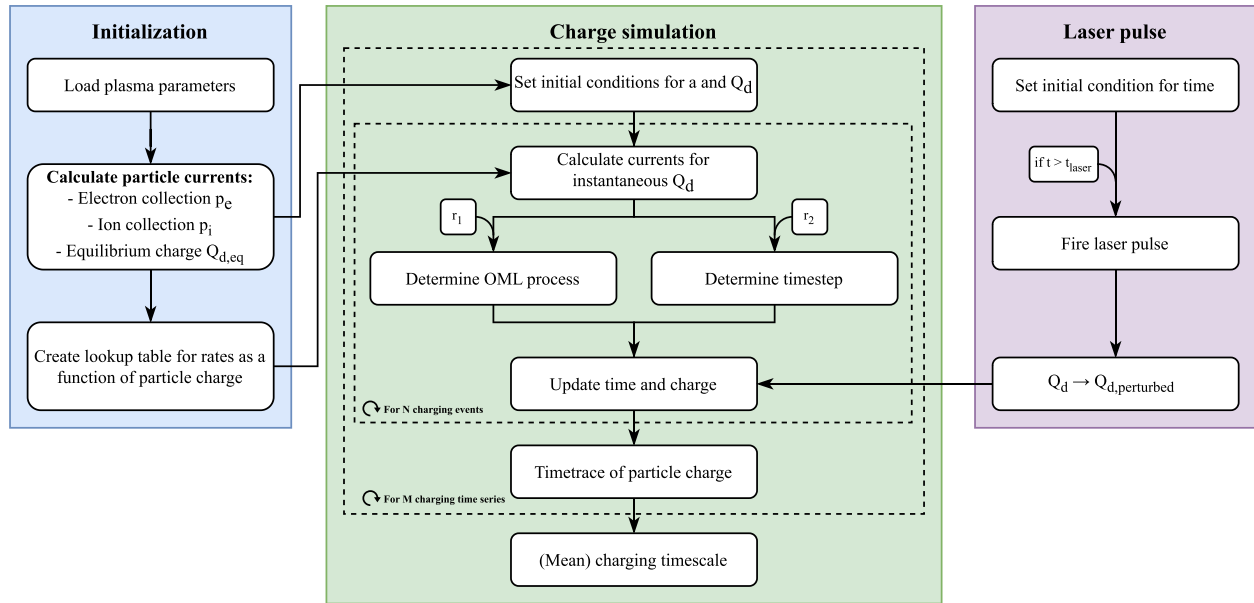
FIG. 1. Schematic overview of the OML charging model for modeling the (de/re)-charging of a nanoparticle in the bulk of a nanodusty plasma. After setting the plasma parameters and constructing a lookup table for the currents in the initialization phase, the charge simulation can start. Using the lookup table, the nanoparticle charge and time are updated. The laser pulse is modeled by instantaneously changing the charge, after which the simulation is resumed. A single time trace consists of $N = 10000$ charging events, and a total of $M = 500$ time traces are averaged to determine the charging timescale.

During a single simulation step, the OML process is determined via a random number $r_1 \in (0, 1)$, such that

$$\begin{cases} \text{OML}_e : Q_d \to Q_d - e, & \text{if } r_1 < (p_e)/(p_e + p_{i+}) \\ \text{OML}_{i+} : Q_d \to Q_d + e, & \text{otherwise.} \end{cases} \quad (5)$$

Here, the determination is based on weighing the electron/ion currents at the instantaneous value of the dust particle charge Q_d. If, in this way, an electron (ion) is collected, the particle charge decreases (increases) by one elementary charge. Subsequently, using a second random number $r_2 \in (0, 1)$, the time between charging events is determined via

$$\Delta t = \frac{-\ln(r_2)}{p_e + p_{i+}}. \quad (6)$$

- After determining the charging process and the timestep, both the dust particle charge and time can be updated. In this way, one obtains a time trace of the dust particle charge $Q_d(t)$. In the simulations shown in this work, the starting condition for the particle charge is the equilibrium charge $Q_{d,eq}$, which is calculated by equating the electron/ion currents and solving for Q_d.
- In the simulation, time and charge are propagated, until the point that the time reaches $t = t_{laser}$. At this point, we simulate laser-induced photodetachment by instantaneously setting the dust charge to $Q_{d,perturbed}$. From there, the model progresses in its usual way until equilibrium is reached again. As input parameters for the model, we choose typical values of the species densities of an (electron-depleted) plasma bulk,[65] i.e., $n_{i+} = 1 \times 10^{16} \text{m}^{-3}$ and $n_e = 1 \times 10^{15} \text{m}^{-3}$. For the temperatures, we choose $T_{i+} = 300 \text{ K}$ and $T_e = 3 \text{ eV}$. Figure 2

shows a time trace of the relative change in charge on a particle with a radius of $a = 100$ nm with respect to the equilibrium charge, i.e., $(Q_d(t) - Q_{d,eq})/|Q_{d,eq}|$, in the case of the total charge removal $(Q_{d,perturbed} \to 0)$. In order to accurately obtain a (re-)charging timescale, we average $M = 500$ time traces and obtain a mean timescale τ. Along with the charge simulation, an exponential fit of the recharging decay is added in blue, of which the timescale is found to be $\tau = 6.39 \mu s$, for the given set of plasma and dust parameters.
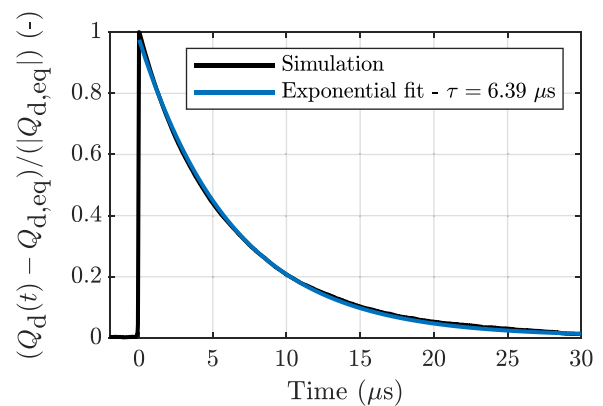
FIG. 2. Time trace of the OML charging model, for a particle with a radius of $a = 100$ nm, suspended in an electron-depleted plasma bulk with $n_{i+} = 1 \times 10^{16} \text{m}^{-3}$, $n_e = 1 \times 10^{15} \text{m}^{-3}$, $T_{i+} = 300 \text{ K}$, and $T_e = 3 \text{ eV}$. In this figure, the black line represents the charge simulations, while the blue line shows an exponential fit for the decay toward equilibrium after total charge removal by UV radiation.

III. EXPERIMENT

Figure 3 shows a top view of the experimental setup, which is similar to the one used in our previous work[24] and will therefore be discussed concisely. Section III A will continue with describing the general equipment and the diagnostics necessary for monitoring the dust growth. In Sec. III B, a more detailed description will be provided about the equipment necessary to measure the additional electron release from the nanoparticles. Finally, Sec. III C explains the experimental procedure and how these diagnostics work together in order to determine the dust particle size.

A. Plasma generation and monitoring of dust growth

Inside the vacuum vessel, a plasma was created in a cylindrical metallic cavity (with a radius of $R_{cav} = 33$ mm and a height of $h_{cav} = 40$ mm) containing a mixture of argon and HMDSO [hexamethyldisiloxane, $(CH_3)_3–Si–O–Si–(CH_3)_3$]. The driving frequency of the plasma was set using a signal generator (Agilent 33250A) to $f = 13.56$ MHz, which delivered a typical input power of $P_{RF} = 21$ W to the plasma. The partial pressures of argon and HMDSO were $p_{Ar} = 6.0$ and $p_{HMDSO} = 0.5$ Pa, respectively. The pressure was regulated using an MKS Type 153 butterfly valve and kept constant during the experiment. The electrical characteristics of the plasma (i.e., RF voltage, current, power, and phase angle) were measured using an Impedans Octiv Poly impedance meter.

Furthermore, a laser ($\lambda = 532$ nm) was used to monitor the dust growth via laser light extinction measurements. The intensity of the laser beam $I(t)$ was measured as a function of time, from which the transmittance $T = I(t)/I_0$, i.e., the ratio between the intensity $I(t)$ and the reference intensity (without dust particles) I_0, was calculated. When dust particles were present in the discharge, a portion of the light would be absorbed or scattered by the particles, which would reduce the transmittance below unity.

Finally, the free electron density of the plasma was monitored using microwave cavity resonance spectroscopy (MCRS). This technique has previously been applied to different types of plasmas.[32,66–68] Using an antenna, low-power ($P_{\mu w} = 40$ mW $\ll P_{RF}$) microwaves with a frequency around that of an eigenmode of the cavity were introduced. Using a Keysight E5063A vector network analyzer (VNA), a frequency sweep was performed and the reflected power was measured with a temporal resolution of approximately 100 ms. In this way, the frequency response of the cavity could be reconstructed and one could determine the eigenfrequency of the cavity by fitting the resonance curve using a Lorentzian line shape. MCRS relies on the fact that the permittivity of the medium inside the cavity changes when a plasma is created. The volume-averaged electron density $\hat{n}_e$ can be determined by measuring the difference $\Delta f = f_{plasma} - f_{vacuum}$ in the eigenfrequency of the cavity between a situation with and without plasma, respectively,[69,70]

$$\hat{n}_e = \frac{8\pi^2 \varepsilon_0 m_e f_{plasma}^2}{e^2 f_{vacuum}} \frac{\Delta f}{V_{plasma-cavity}}. \tag{7}$$

In this equation, $V_{plasma-cavity}$ is the (electric-field-squared-weighted) volume ratio, which expresses the ratio between the plasma volume V_{plasma} and the cavity volume V_{cavity}, defined as follows:

$$V_{plasma-cavity} = \frac{\iiint_{V_{plasma}} |\mathbf{E}|^2 d\mathbf{r}}{\iiint_{V_{cavity}} |\mathbf{E}|^2 d\mathbf{r}}. \tag{8}$$

Using a numerical model in COMSOL Multiphysics, the electric field of the TM_{010} mode is simulated by solving Maxwell's equations in a cylindrical cavity, so that the integrals can be evaluated numerically.[24] Similar to our previous work,[32] electron densities can be measured
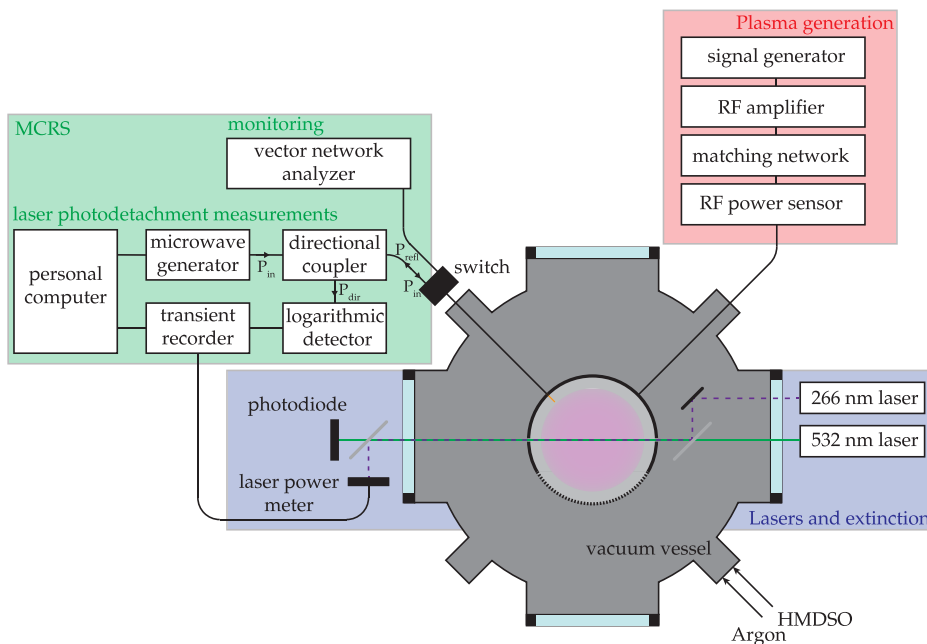
FIG. 3. Schematic of the experimental setup used for the measurements described in this work. A low-pressure nanodusty Ar/HMDSO plasma is created in a cylindrical cavity. The plasma is electrically characterized using an impedance meter, the extinction of green laser light by the dust particles is measured using a photodiode, and the free electron density is measured using MCRS. For the fast photodetachment measurements, a microwave generator and a transient recorder are used to measure the additional electron density released by an ultraviolet laser.

with a typical accuracy of around 1%, as found by error propagation of the parameters of the Lorentzian fit.

B. Measuring the release of electrons from dust particles by laser-induced photodetachment

This section describes the equipment necessary for performing the laser-induced photodetachment measurements. Using a Quantel Big Sky Ultra laser, short (pulse time $t_{pulse} \approx 8$ ns) ultraviolet (wavelength $\lambda = 266$ nm and diameter $D_{laser} = 2$ mm) laser pulses were sent through the cavity via two parallel slits in the sidewall of the cavity with a repetition frequency of $f_{laser} = 20$ Hz. The mean laser pulse energy during the experiment was measured to be $E_{pulse} = 333\,\mu J$, which results in a laser fluence of $F = E_{pulse}/A_{laser} \approx 100$ J/m^2. In comparison with incandescence experiments described in the literature,[60,71] where the laser fluence is typically one order of magnitude higher, it may be concluded that heating of the particles is not dominant in our experiments. However, the energy of the photons ($E = hc/\lambda = 4.66$ eV) is enough to overcome the work function of the electrons attached to the dust particles and, hence, to release electrons from the particles' surfaces upon irradiation. The additional free electrons due to the photodetachment processes can be measured using MCRS. As the time resolution of this process is much faster than the time resolution of the vector network analyzer, another system is required in order to be able to follow these fast transient processes. Using a combination of a Stanford Model SG386 microwave generator and a Spectrum M3i.4121-exp transient recorder, the response of the cavity for a single microwave frequency can be sampled with a temporal resolution down to $t_{TR} = 4$ ns. During the measurement, the microwave generator sets a frequency near the eigenfrequency of the cavity, and the transient recorder measures N_{av} individual time traces (and therefore probing the same amount of laser pulses) before setting the next microwave frequency. In this way, a frequency sweep (consisting of N_{freq} distinct frequencies) is made to reconstruct the resonance curve, consisting of a total of $N_{meas} = N_{freq} \times N_{av}$ individual laser pulses. Similar to what was described in Sec. III A, the electron density is calculated from determining the peak position of the resonance curve using Eq. (7), before, during, and after the laser pulse. One should note that, in order to correctly represent the additional volume-averaged electron density induced by the laser beam Δn_e, some adaptations have to be made to Eqs. (7) and (8). First, instead of looking at the shift between the plasma and the vacuum condition, we are now looking at the shift during the time period before and after the laser is fired. Second, the volume ratio now needs to incorporate the volumes of the laser compared to that of the cavity, such that

$$\Delta n_e = \frac{8\pi^2\varepsilon_0 m_e f_{plasma+laser}^2}{e^2 f_{plasma}} \frac{\Delta f}{V_{laser-cavity}},$$

with

$$V_{laser-cavity} = \frac{\iiint_{V_{laser}} |\mathbf{E}|^2 d\mathbf{r}}{\iiint_{V_{cavity}} |\mathbf{E}|^2 d\mathbf{r}}. \quad (9)$$

Note that in this equation, the disturbance in the cavity is now caused by the UV laser, which implies that the frequency shift $\Delta f = f_{plasma+laser} - f_{plasma}$ is calculated with respect to eigenfrequency just before the laser pulse is fired.

Additionally, one should note that the raw data from the transient recorder has been filtered with a low-pass filter with an upper frequency of 10 MHz, in order to remove additional noise coming from the driving frequency of the plasma ($f = 13.56$ MHz).

C. Experimental procedure

This section explains the procedure in which the aforementioned diagnostics are used in experiments. The aims are to (i) monitor dust growth in a low-pressure Ar/HMDSO nanodusty plasma and subsequently (ii) to perform laser-induced photodetachment measurements on a formed dust cloud. Figure 4 shows a schematic timing overview of the applied experimental procedure. The experiment consists of three stages: the growth stage (G), the settle stage (S), and the measurement stage (M). Furthermore, the three rows (plasma, monitoring, and photodetachment) each consist of a number of properties or diagnostics, which are present in the experimental setup. Horizontally, Fig. 4 shows in which measurement stage each of the diagnostics is active.

In the beginning of the growth stage (G), the plasma is switched on (at $t = 0$s) in a mixture of argon and HMDSO by applying RF power. This plasma and the formation of dust are monitored using the three diagnostics mentioned in Sec. III A. At $t = 80$ s, the HMDSO inlet valve closes, which leads to the termination of dust growth, as no precursor gas is fed into the discharge volume anymore. Note that the already grown cloud of nanoparticles will remain confined in the discharge.

During the settle stage (S), the system gets one minute to respond to the closing of the HMDSO valve. During this period, the pressure slightly drops from $p_{Ar+HMDSO} = 6.5$ to $p_{Ar} = 6.0$ Pa. Note that it is likely that a substantial amount of negative ions is still trapped in the discharge even though the HMDSO inlet is terminated. The remaining situation is now an argon plasma containing a cloud of nanoparticles, with additional negative ions from the growth stage. It is assumed that the dust particles no longer continue growing after the settle stage has
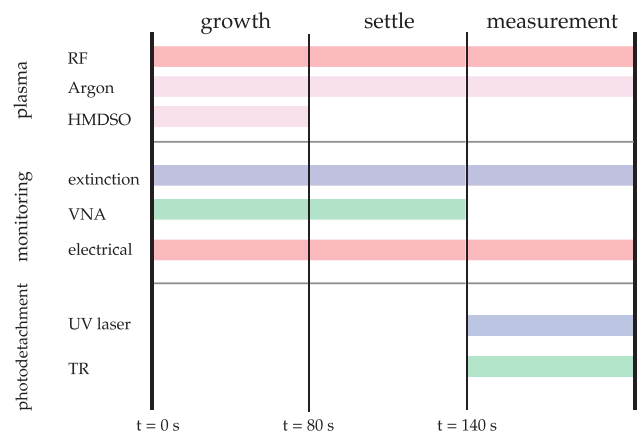
FIG. 4. Schematic of the experimental procedure. From $t = 0$ s until $t = 80$ s, dust particles are growing in the plasma, while the plasma-dust system is monitored by means of laser light extinction, electron density measurements using the VNA, and by electrical characterization. After switching off the HMDSO flow at $t = 80$ s, the system gets one minute to settle and adapt to the slight change in pressure. After that, the pulsed UV laser is switched on and the photodetached electron density is measured using a microwave generator and a transient recorder (TR).

ended, so that we are doing photodetachment measurements on a stationary sample of dust particles. Also during this stage, the dust growth is monitored by means of laser light extinction measurements, by measurements of the free electron density by the network analyzer, and by electrical characterization. This is done in order to verify that the plasma parameters stabilize before the end of the settle stage.

During the measurement stage (M), the laser-induced photodetachment measurements are conducted. From this moment, the UV laser starts pulsing with a repetition frequency of $f_{laser} = 20$ Hz and the MCRS system is switched from the VNA to the microwave generator and the transient recorder. In this way, the fast transient response of the free electron density due to the laser-induced photodetachment can be measured. As explained in Sec. III B, a single measurement consists of measuring the temporal response of the cavity to microwaves around its resonance frequency. In post-processing, the resonance curve is reconstructed, from which a time series of the electron density can be determined. In doing these measurements, it is implicitly assumed that during the total measurement time (typically in the order of 1–2 min), both the plasma and the dust sample remain stationary in time so that every laser pulse probes a similar plasma-dust system. Furthermore, it is assumed that the UV laser does not influence the plasma and the dust cloud. These assumptions are verified by monitoring both the electrical parameters of the plasma and the extinction of laser light by the dust cloud.

IV. RESULTS AND DISCUSSION

This section will discuss the results of the experiments leading to the measurement of the dust particle size in a nanodusty plasma using laser-induced photodetachment and measurements of the temporal evolution of the additional free electron density. In Sec. IV A, we start with showing results of the growth (G) and settle (S) stages (as shown in Fig. 4). The section continues with showing a typical result of the subsequent laser-induced photodetachment measurement (M), from which the charging timescale can be deducted. Section IV B continues with using the OML model from Sec. II to connect the charging timescale to the dust particle size and shows SEM measurements for comparison. Then, in Sec. IV C, we discuss the sensitivity of the OML model to its input plasma parameters, such as the positive ion density. Finally, Sec. IV D proposes the idea to apply the method in a reversed fashion to determine the positive ion density instead, using the dust particle size data from the SEM measurements.

A. Laser-induced photodetachment on a nanodusty plasma

Figure 5 shows the results of the monitoring measurements of the free electron density using the VNA [from Eq. (7)] and the transmittance of the 532 nm laser light as a function of time, during the growth stage, the settle stage, and the measurement stage. These two measurements were used to monitor the dust growth and are very similar to the experiments in our earlier work.[32] The main observations will be briefly reiterated here. During the growth stage ($t \leq 80$ s), we see (in the upper panel of Fig. 5) that the electron density remains constant during the first half and suddenly drops around $t = 55$ s. This corresponds to the coagulation phase mentioned in the Introduction as dust particles then tend to collect free electrons from the plasma and therefore charge negatively. In this measurement, we observe a drop in the free electron density of around a factor 10. Simultaneously,
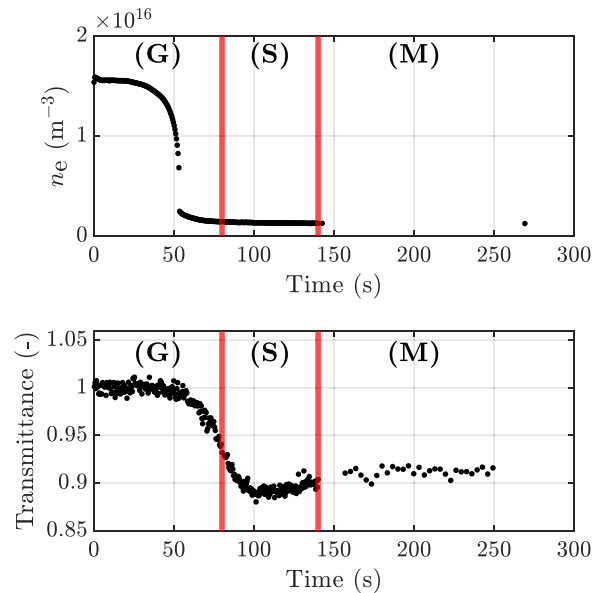

FIG. 5. Results of the monitoring experiments. The free electron density and the transmittance were monitored during 80 s of dust growth (G), 60 s of settling (S), and during the measurement stage (M). The presence of dust particles is shown in the form of the sharp decrease in the electron density as well as the decrease in the transmittance.

as can be seen in the second panel of Fig. 5, we see that after coagulation, the transmittance starts to decrease below unity. This trend is a sign of dust particles being present in the discharge: A part of the light is absorbed or scattered by the dust cloud (which lowers the transmittance), as also described in our previous work.[32]

After switching off the HMDSO flow at $t = 80$ s, we observe that the electron density remains approximately constant during the settle stage, while the transmittance still shows changes. This is most probably due to the redistribution of dust particles over the discharge and the slight pressure drop after the precursor gas source is terminated. Eventually, the signal stabilizes in time, such that during the measurement stage, we are probing a stationary dust sample. The transmittance is also monitored during the measurement stage, such that the stationarity of the dust sample can be qualitatively verified.

Figure 6 shows the result of the laser-induced photodetachment measurement on the dust cloud (corresponding to the measurement stage in Fig. 4). Using the microwave generator and the transient recorder, the resonance peak was constructed, from which the eigenfrequency was found from a Lorentzian fit. Using Eq. (7), the shift in the eigenfrequency is then translated into a released electron density. From this measurement, we can qualitatively describe the transient behavior of the electron density in three stages: (i) Before the laser pulse ($t < 0$ μs), the plasma is in an equilibrium situation, which is the reference case. The laser pulse is fired at $t = 0$ μs, indicated by the sharp increase in the free electron density (ii). This moment in time corresponds to the laser-induced photodetachment, where electrons are released from the dust particles and subsequently contribute to an increase in the free electron density of the plasma. The timescale of the increase in the signal is around $\tau_{rise} \sim 50$ ns, which corresponds to the
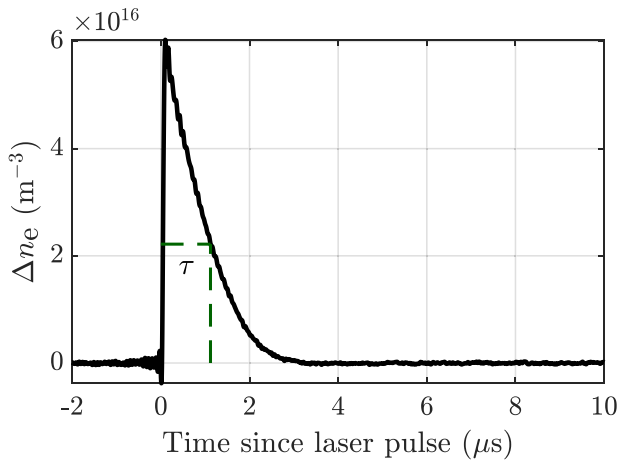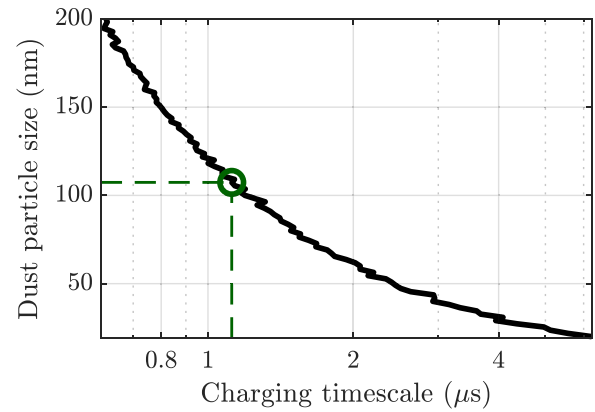
FIG. 6. The photo-released electron density as a function of time. At $t = 0$ s, the laser pulse was fired, after which the free electron density rapidly increases. It is followed by a decay of the electron density back to its equilibrium value. The recharging time is defined as the $1/e$-time of the decay. In this measurement, the decay was measured as $\tau_{meas} = 1.12 \pm 0.04\,\mu s$.


FIG. 7. Simulation results of the charging timescale as a function of dust particle size. For the experimentally measured decay timescale of $\tau_{meas} = 1.12 \pm 0.04\,\mu s$, a dust particle size of $a = 107 \pm 6$ nm is obtained. For the simulations, plasma parameters of $n_e = 1.4 \times 10^{15} m^{-3}$, $n_{i+} = 5n_{e0} = 9.0 \times 10^{16} m^{-3}$, $T_e = 3$ eV, and $T_{i+} = 300$ K were used.

characteristic response timescale of the cavity, as calculated from the width of the resonance mode.[24] This indicates that even though the transient recorder can sample faster ($t_{TR} = 4$ ns), the cavity timescale is limiting for following physical phenomena. After this, we observe (iii) the relaxation of the free electron density, back to the reference position, within a timescale of a few microseconds.

The decay timescale of the electron density in Fig. 6 is the main quantity of interest in these measurements, as this quantity can be directly compared to the charging timescale calculated with the OML model in Sec. II. Similar to the work of Cui and Goree,[63] we define the charging time τ_{meas} to be the $1/e$-time of the decay. In Fig. 6, for this particular measurement, this corresponds to a decay time of $\tau_{meas} = 1.12 \pm 0.04\,\mu s$, as indicated by the dark green dashed line. The error in this value arises from propagation of the error in Δn_e, which comes from the 95% confidence interval of the fitting parameters of the Lorentzian line shape fit.

B. Determining the dust particle size

From Fig. 6, we obtained an experimentally measured timescale for the recharging of nanoparticles in a nanodusty plasma after their surface charge is (partially) removed by laser-induced photodetachment. This section will use the charging model explained in Sec. II to determine the dust particle size by modeling this recharging timescale using the OML framework. Figure 7 shows the simulation results of the charging timescale determination as a function of the dust particle size. Each point in the graph represents the average charging timescale over $M = 500$ time traces with a fixed dust particle size. In this case, the assumed plasma temperatures were $T_e = 3$ eV and $T_{i+} = 300$ K, based on typical values in a low-pressure RF-driven plasma.[65] Furthermore, the electron density at the time of the measurement was $n_e = 1.4 \times 10^{15} m^{-3}$, as experimentally obtained using MCRS. The positive ion density was assumed to be five times larger than the initial electron density, i.e., $n_{i+} = 5n_{e0} = 9.0 \times 10^{16} m^{-3}$, similar to what is typically found in modeling efforts of dusty plasmas, taking into

account the presence of negative ions.[38,72,73] The impact of the assumptions for the electron temperature and the positive ion density will be discussed in more detail in Sec. IV C. Figure 7 shows that with increasing particle size from $a = 20$ to $a = 200$ nm, the charging timescale decreases from $\tau = 6.2$ to $\tau = 0.62\,\mu s$. Using the created lookup-table that relates the charging timescale to the dust particle size, we find that using the measured timescale of $\tau_{meas} = 1.12 \pm 0.04\,\mu s$, the expected dust particle size is found to be $a = 107 \pm 6$ nm, as indicated by the dark green marker. Here, the error in the dust particle size rises from the error in the measured charging timescale τ_{meas}.

An appropriate next step would be to verify the newly developed method by cross-checking it with an already established particle sizing method. The most straightforward method to verify the dust particle size is *ex situ* scanning electron microscopy (SEM). After switching off the plasma, the particles are no longer confined in the plasma bulk and will fall down and leave the discharge region. Directly below the discharge, we placed SEM substrates, covered with double-sided carbon tape. In this way, the same sample of particles of which we determined the size using the decay of the additional electron density can be measured using SEM. Figure 8 shows one of the SEM images which were made, along with orange circular markers to indicate the particles. Subsequently, a MATLAB script was developed to detect the edges of the particles and determine the size from the particle boundaries. By also analyzing a pristine sample that has not seen a plasma or dust particles, it was verified that the additional small (cauliflower-shaped) white spots in the image are due to the structure of the carbon tape.

Analyzing multiple SEM pictures, the size of $N = 173$ particles has been measured. Figure 9 shows the obtained particle size distribution (PSD) from these images by the light blue histogram. Since the particle size distribution of particles grown in a nanodusty plasma is expected to be lognormal,[51] a fit of the PSD is included in blue. The distribution has a mean of $\mu_{SEM} = 116$ nm and a standard deviation of $\sigma_{SEM} = 13$ nm. We can see that there is good agreement between the dust particle size predicted with the newly developed PD decay
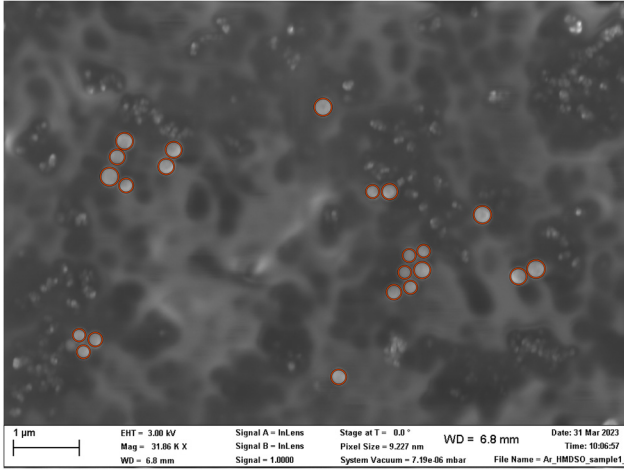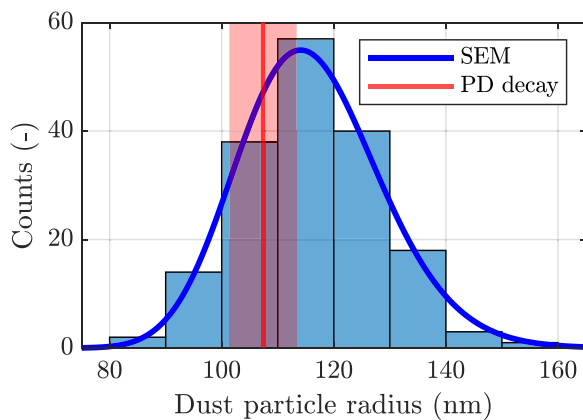
FIG. 8. Scanning electron microscope (SEM) image of the dust particles of which the size has been determined during the photodetachment experiment. The small cauliflower-shaped structures are due to the structure of the carbon tape.

method (the red region in Fig. 9) and the observed particle size from the SEM measurements.

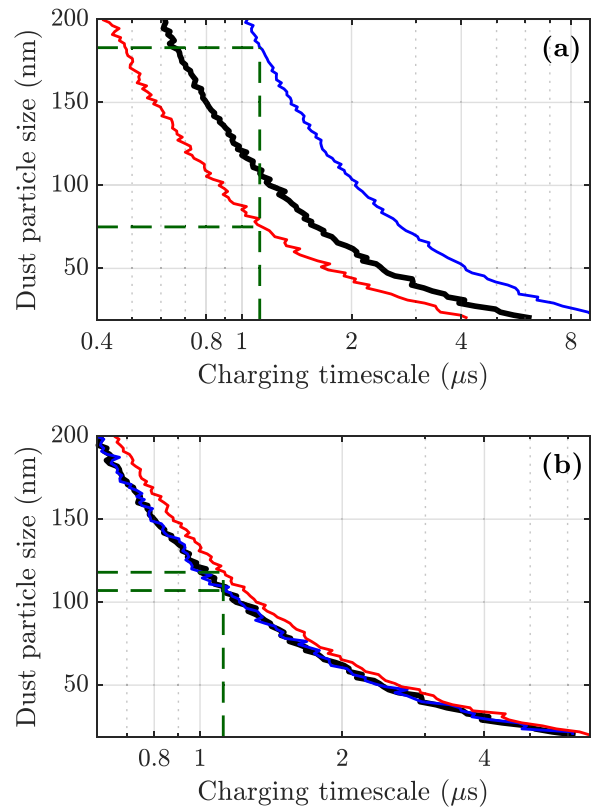### C. Sensitivity analysis of the OML model to the positive ion density

Although Fig. 9 shows good agreement between the predicted dust particle size and the particle size measured by SEM, it would still be good practice to reflect on the newly developed method. As described in Sec. II, we use the OML theory to describe the charging of nanoparticles by the collection of charged species. In this section, the most stringent assumptions in the model are identified and a sensitivity analysis is performed to investigate the consequences of the assumptions. The charging behavior of the dust particles in a plasma

heavily depends on the plasma parameters, i.e., the densities and temperatures of the free electrons and the positive ions. From these four parameters, only two of these are well determined: the electron density n_e is measured with MCRS and the positive ion temperature generally remains close to room temperature for typical low-pressure RF plasmas, as the driving frequency of the plasma is higher than the ion plasma frequency. From the remaining two plasma parameters, the charging time is most sensitive to the positive ion density n_{i+}.

In order to assess the sensitivity to the other two parameters, Fig. 10 shows two additional sets of OML simulations which were performed. The procedure was similar to the one shown in Fig. 7. Again, for each particle size, we have performed $M = 500$ time traces and calculated the average charging timescale. The upper panel of the figure deals with the sensitivity in the positive ion density n_{i+}. Here, the central black curve shows the reference case, using $n_{i+} = n_{i+,ref} = 5n_{e0}$. In order to illustrate the sensitivity, we have added charging timescale curves for an increased ($+50\%$, i.e., $n_{i+} = 1.5n_{i+,ref}$) and decreased (-50%, i.e., $n_{i+} = 0.5n_{i+,ref}$) positive ion density n_{i+}. When increasing (decreasing) the positive ion density with respect to the reference case, the curve will shift toward the red (blue) curve in the figure. In

FIG. 9. Particle size distribution obtained from SEM images. A lognormal distribution fit with a mean of $\mu_{SEM} = 116$ nm and a standard deviation of $\sigma_{SEM} = 13$ nm is shown in red. There is good agreement between the found distribution and the predicted dust particle size using the photodetachment decay method, predicting $a = 107 \pm 6$ nm.

FIG. 10. Sensitivity analysis of the OML model to the positive ion density (a) and the electron temperature (b). In panel (a), the thick black curve represents the reference case, where $n_{i+} = n_{i+,ref} = 5n_{e0}$. The red (blue) region indicates the direction of change when increasing (decreasing) the positive ion density to $n_{i+} = 1.5n_{i+,ref}$ ($n_{i+} = 0.5n_{i+,ref}$). Similarly, in panel (b), the effect of the electron temperature is shown after increasing or decreasing it with 50% with respect to the reference case of $T_e = T_{e,ref} = 3$ eV.

general, for any fixed value of the dust particle size, the charging timescale decreases with increasing positive ion density. This comes from the fact that with a higher positive ion density, the equilibrium charge of the particles becomes less negative. As already predicted in the first implementation of the stochastic OML model,[63] the charging timescale is inversely proportional to the plasma density. Furthermore, solving the differential equation (4) analytically[24,74] showed similar behavior.

The upper panel of Fig. 10 shows that the method is indeed sensitive to the positive ion density: For the measured decay time of $\tau_{meas} = 1.12 \pm 0.04\,\mu s$, varying the ion density from $n_{i+} = 0.5 n_{i+,ref}$ to $n_{i+} = 1.5 n_{i+,ref}$ leads to finding a dust particle size ranging from $a = 183$ to 75 nm, respectively. In the current experimental approach, measuring the positive ion density is far from straightforward: It generally requires complex techniques such as mass spectrometry and/or direct access to the plasma bulk, which is currently limited by the microwave cavity.

The lower panel of Fig. 10 shows a similar sensitivity analysis for variation of the electron temperature. In a similar fashion, we have chosen a reference electron temperature of $T_e = T_{e,ref} = 3\,eV$. Next, we have run additional simulations for an increased ($T_e = 1.5 T_{e,ref}$) and a decreased ($T_e = 0.5 T_{e,ref}$) electron temperature. From this figure, it is clear that the effect of varying the electron temperature is indeed smaller: Increasing (decreasing) the electron temperature leads to finding a dust particle size in the range of $a = 107$–118 nm.

D. Using the dust particle size measured by SEM to estimate the positive ion density

Section IV C shows that the OML model is most sensitive to the positive ion density n_{i+}. In this section, we will propose the idea of reversing the proposed method and using the dust particle size obtained from the SEM measurements as an input for the OML charging model and determining the positive ion density instead. In this way, we can use the OML model of Sec. II to calculate the charging timescale, but this time while using the measured particle size distribution, and varying the positive ion density n_{i+}. In such a simulation, the particle size distribution is divided into $N_{sec} = 30$ sections. For each of these particle sizes, an OML simulation similar to the one in Fig. 2 is performed. Then, a total OML simulation time trace is constructed by weighing each of the separate simulations by the particle size distribution obtained by the SEM measurements. Finally, the decay timescale of this simulation is determined using an exponential fit. Subsequently, the process is repeated for a different positive ion density. Figure 11 shows the results of the parameter sweep in the positive ion density, in showing the relation between the positive ion density and the calculated charging timescale. We can now determine the positive ion density by using the experimentally measured charging timescale $\tau_{meas} = 1.12 \pm 0.04\,\mu s$. In this way, we find a positive ion density of $n_{i+} = (8.4 \pm 0.4) \times 10^{16}\,m^{-3}$. To put this value in perspective, it is 4.6 times as large as the initial electron density measured by MCRS, i.e., $n_{i+} = 4.6 n_{e0}$. This is in accordance with what was expected from models in these types of plasmas.[38,72,73] This implies that instead of making an assumption for the positive ion density n_{i+} and determining the dust particle size a (as shown in the sections leading up to Sec. IV B), the method can also be used to determine the positive ion density n_{i+}, in the case that the dust particle size is known
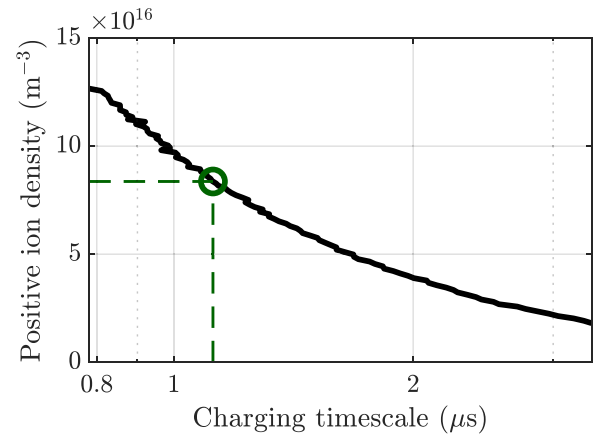

FIG. 11. Determination of the positive ion density using the dust particle size distribution obtained from SEM measurements. Using the experimentally measured charging timescale $\tau_{meas} = 1.12 \pm 0.04\,\mu s$, a positive ion density of $n_{i+} = 8.4 \pm 0.4 \times 10^{16}\,m^{-3} = 4.6 n_{e0}$ was obtained.

(for example, by SEM). From such a method, both modeling efforts and theory development could greatly benefit.

V. CONCLUSIONS

This work presents a novel method to determine the mean dust particle size from the decay of the additional electron density upon interaction with a UV laser. The electron density in the plasma was measured using MCRS. By using the combination of a microwave generator and a transient recorder, the electron density could be measured with a resolution of 250 MHz. The timescale with which the electron density decays back to the reference position is directly related to the charging time of the dust particles. The charging time of a dust particle in a plasma depends on the governing plasma parameters and on the dust particle size, and this quantity can be determined using a stochastic model based on the OML theory. Comparison of the measured decay timescale to the charging timescale yields the (mean) dust particle size of the sample. In its current form, this method is applicable to low-pressure nanodusty plasmas. However, if one wants to apply the method to higher pressures, the OML positive ion current should be adapted for the increased collisionality.[75]

Using this method for a proof of principle measurement, it was found that for our experimental conditions, we have grown dust particles with an expected radius of $a = 107 \pm 6\,nm$. This value is not only similar to the results of other experiments in the literature,[47,62,76] but also matched *ex situ* SEM measurements of the same sample quite well ($a_{SEM} = 116 \pm 13\,nm$). Furthermore, we established that the charging timescale from the OML model is most sensitive to the input positive ion density. It was also shown that using the value of the size from the SEM measurements, the positive ion density in the experiment was estimated to be 4.6 times as large as the initial electron density, which is typical for nanodusty (electronegative) plasmas.

In conclusion, our newly developed method shows promising results for the determination of the dust particle size in a nanodusty plasma. On top of this, the method is minimally invasive since the UV laser power does not necessarily need to be high, in contrast to typical photodetachment experiments where it is necessary to operate in the

saturation regime. Using this method to investigate the dust particle size in a nanodusty plasma can be beneficial for fundamental research and industrial applications and ultimately for comparison with dusty plasma modeling efforts.

ACKNOWLEDGMENTS

AUTHOR DECLARATIONS
Conflict of Interest

The authors have no conflicts to disclose.

Author Contributions

Tim Jacobus Maria Donders: Data curation (lead); Formal analysis (lead); Investigation (lead); Methodology (equal); Software (lead); Validation (lead); Visualization (lead); Writing – original draft (lead). **Tim Jacobus Adrianus Staps:** Formal analysis (supporting); Methodology (equal); Validation (equal); Writing – review & editing (equal). **Job Beckers:** Conceptualization (lead); Funding acquisition (lead); Project administration (lead); Supervision (lead); Writing – review & editing (equal).

DATA AVAILABILITY

The data that support the findings of this study are available from the corresponding author upon reasonable request.

REFERENCES

[1]A. Melzer, *Lecture Notes in Physics* (Springer, Cham, 2019), Vol. 962.

[2]A. Piel, *Plasma Physics: An Introduction to Laboratory, Space and Fusion Plasmas*, 2nd ed. (Springer, 2017).

[3]C. K. Goertz, "Dusty plasmas in the solar system," Rev. Geophys. **27**, 271–292, https://doi.org/10.1029/RG027i002p00271 (1989).

[4]A. Bouchoule, *Dusty Plasmas: Physics, Chemistry, and Technological Impacts in Plasma Processing* (John Wiley & Sons, 1999).

[5]T. Takeuchi and D. N. C. Lin, "Radial flow of dust particles in accretion disks," Astrophys. J. **581**, 1344–1355 (2002).

[6]S. A. Collins, A. F. Cook, J. N. Cuzzi, G. E. Danielson, G. E. Hunt, T. V. Johnson, D. Morrison, T. Owen, J. B. Pollack, B. A. Smith, and R. J. Terrile, "First Voyager view of the rings of Saturn," Nature **288**(5790), 439–442 (1980).

[7]A. A. Simon, M. M. Hedman, P. D. Nicholson, M. S. Tiscareno, M. R. Showalter, T. McDonald, and S. Callos, "Hubble detects the start of a new Saturn ring spoke season," Geophys. Res. Lett. **50**, e2022GL101904, https://doi.org/10.1029/2022GL101904 (2023).

[8]M. A. van de Kerkhof, J. P. Benschop, and V. Y. Banine, "Lithography for now and the future," Solid-State Electron. **155**, 20–26 (2019).

[9]M. Van De Kerkhof, A. M. Yakunin, V. Kvon, A. Nikipelov, D. Astakhov, P. Krainov, and V. Banine, "EUV-induced hydrogen plasma and particle release," Radiat. Eff. Defects Solids **177**, 486–512 (2022).

[10]G. S. Selwyn, "Optical characterization of particle traps," Plasma Sources Sci. Technol. **3**, 340–347 (1994).

[11]B. van Minderhout, T. Peijnenburg, P. Blom, J. M. Vogels, G. M. W. Kroesen, and J. Beckers, "The charge of micro-particles in a low pressure spatial plasma afterglow," J. Phys. D **52**, 32LT03 (2019).

[12]B. Van Minderhout, J. C. A. Van Huijstee, B. Platier, T. Peijnenburg, P. Blom, G. M. W. Kroesen, and J. Beckers, "Charge control of micro-particles in a shielded plasma afterglow," Plasma Sources Sci. Technol. **29**, 11 (2020).

[13]J. C. A. Van Huijstee, P. Blom, and J. Beckers, "Position dependent microparticle charge in a spatiotemporal afterglow plasma," J. Appl. Phys. **30**, 33704 (2023).

[14]H. Thomas, G. E. Morfill, V. Demmel, J. Goree, B. Feuerbacher, and D. Möhlmann, "Plasma crystal: Coulomb crystallization in a dusty plasma," Phys. Rev. Lett. **73**, 652 (1994).

[15]N. Chaubey and J. Goree, "Preservation of a dust crystal as it falls in an afterglow plasma," Front. Phys. **10**, 479 (2022).

[16]R. Banka, K. Vermillion, L. Matthews, T. Hyde, and L. Couëdel, "Dependence of ion wake characteristics on experimental conditions," Plasma Phys. Controlled Fusion **65**, 044006 (2023).

[17]H. M. Thomas and G. E. Morfill, "Melting dynamics of a plasma crystal," Nature **379**(6568), 806–809 (1996).

[18]A. A. Mamun and P. K. Shukla, "Discoveries of waves in dusty plasmas," J. Plasma Phys. **77**, 437–455 (2011).

[19]B. Tadsen, F. Greiner, S. Groth, and A. Piel, "Self-excited dust-acoustic waves in an electron-depleted nanodusty plasma," Phys. Plasmas **22**, 113701 (2015).

[20]A. Melzer, H. Krüger, S. Schütt, and M. Mulsow, "Dust-density waves in radio-frequency discharges under magnetic fields," Phys. Plasmas **27**, 33704 (2020).

[21]T. W. Hyde, J. Kong, and L. S. Matthews, "Helical structures in vertically aligned dust particle chains in a complex plasma," Phys. Rev. E **87**, 053106 (2013).

[22]P. Meijaard, T. J. Staps, and J. Beckers, "Step-wise excitation for the determination of the resonance frequency of a microparticle confined in a low pressure plasma," Phys. Plasmas **28**, 083502 (2021).

[23]H. Jung, F. Greiner, O. H. Asnaz, J. Carstensen, and A. Piel, "Resonance methods for the characterization of dust particles in plasmas," J. Plasma Phys. **82**, 615820301 (2016).

[24]T. J. A. Staps, T. J. M. Donders, B. Platier, and J. Beckers, "*In-situ* measurement of dust charge density in nanodusty plasma," J. Phys. D **55**, 08LT01 (2021).

[25]S. Groth, F. Greiner, and A. Piel, "Spatio-temporally resolved investigations of layered particle growth in a reactive argon-acetylene plasma," Plasma Sources Sci. Technol. **28**, 115016 (2019).

[26]F. M. J. H. Van De Wetering, R. J. C. Brooimans, S. Nijdam, J. Beckers, and G. M. W. Kroesen, "Fast and interrupted expansion in cyclic void growth in dusty plasma," J. Phys. D **48**, 035204 (2015).

[27]F. M. J. H. Van De Wetering, J. Beckers, and G. M. W. Kroesen, "Anion dynamics in the first 10 milliseconds of an argon-acetylene radio-frequency plasma," J. Phys. D **45**, 485205 (2012).

[28]Z. Marvi, E. Von Wahl, T. Trottenberg, and H. Kersten, "Spatiotemporal sampling of growing nanoparticles in an acetylene plasma," J. Appl. Phys. **127**, 173301 (2020).

[29]J. Beckers and G. M. W. Kroesen, "Gas temperature dependence of coagulation onset times for nanoparticles in low pressure hydrocarbon plasmas," Appl. Phys. Lett. **103**, 123106 (2013).

[30]J. Berndt, S. Hong, E. Kovačević, I. Stefanović, and J. Winter, "Dust particle formation in low pressure Ar/CH_4 and Ar/C_2H_2 discharges used for thin film deposition," Vacuum **71**, 377–390 (2003).

[31]A. Bouchoule and L. Boufendi, "Particulate formation and dusty plasma behaviour in argon-silane RF discharge," Plasma Sources Sci. Technol. **2**, 204 (1993).

[32]T. J. M. Donders, T. J. A. Staps, and J. Beckers, "Characterization of cyclic dust growth in a low-pressure, radio-frequency driven argon-hexamethyldisiloxane plasma," J. Phys. D **55**, 395203 (2022).

[33]B. Despax, K. Makasheva, and H. Caquineau, "Cyclic powder formation during pulsed injection of hexamethyldisiloxane in an axially asymmetric radiofrequency argon discharge," J. Appl. Phys. **112**, 093302 (2012).

[34]R. Wallimann, C. Roth, and P. Rudolf von Rohr, "Nanoparticle production from HMDSO in atmospheric pressure argon-oxygen plasma," Plasma Processes Polym. **15**, 1700202 (2018).

[35]V. Garofano, R. Bérard, S. Boivin, C. Joblin, K. Makasheva, and L. Stafford, "Multi-scale investigation in the frequency domain of Ar/HMDSO dusty plasma with pulsed injection of HMDSO," Plasma Sources Sci. Technol. **28**, 055019 (2019).

[36]Y. Y. Ji, Y. C. Hong, S. H. Lee, S. D. Kim, and S. S. Kim, "Formation of superhydrophobic and water-repellency surface with hexamethyldisiloxane (HMDSO) coating on polyethyleneteraphtalate fiber by atmosperic pressure plasma polymerization," Surf. Coat. Technol. **202**, 5663–5667 (2008).

05 September 2023 12:33:15

[37]R. Bérard, K. Makasheva, H. Sabbah, K. Demyk, and C. Joblin, "Using cold plasma to investigate the mechanisms involved in cosmic dust formation: Role of the C/O ratio and metals," in Proceedings IAU Symposium No. 350, 2019).

[38]K. De Bleecker, A. Bogaerts, and W. Goedheer, "Detailed modeling of hydrocarbon nanoparticle nucleation in acetylene discharges," Phys. Rev. E **73**, 026405 (2006).

[39]D. Herrebout, A. Bogaerts, R. Gijbels, W. J. Goedheer, and A. Vanhulsel, "A one-dimensional fluid model for an acetylene RF discharge: A study of the plasma chemistry," IEEE Trans. Plasma Sci. **31**, 659–664 (2003).

[40]S. Stoykov, C. Eggs, and U. Kortshagen, "Plasma chemistry and growth of nanosized particles in a C_2H_2 RF discharge," J. Phys. D **34**, 2160 (2001).

[41]K. De Bleecker, A. Bogaerts, and W. Goedheer, "Modelling of nanoparticle coagulation and transport dynamics in dusty silane discharges," New J. Phys. **8**, 178 (2006).

[42]P. Agarwal and S. L. Girshick, "Sectional modeling of nanoparticle size and charge distributions in dusty plasmas," Plasma Sources Sci. Technol. **21**, 055023 (2012).

[43]P. Agarwal and S. L. Girshick, "Numerical modeling of an RF argon-silane plasma with dust particle nucleation and growth," Plasma Chem. Plasma Process. **34**, 489–503 (2014).

[44]S. J. Warthesen and S. L. Girshick, "Numerical simulation of the spatiotemporal evolution of a nanoparticle-plasma system," Plasma Chem. Plasma Process. **27**, 292–310 (2007).

[45]U. Kortshagen and U. Bhandarkar, "Modeling of particulate coagulation in low pressure plasmas," Phys. Rev. E **60**, 887–898 (1999).

[46]S. L. Girshick, "Particle nucleation and growth in dusty plasmas: On the importance of charged-neutral interactions," J. Vac. Sci. Technol., A **38**, 011001 (2020).

[47]M. Dworschak, O. H. Asnaz, and F. Greiner, "A minimally invasive electrostatic particle extractor for nanodusty plasmas and its application for the verification of *in situ* Mie polarimetry," Plasma Sources Sci. Technol. **30**, 035011 (2021).

[48]S. Wohlfahrt and D. Block, "High-precision *in situ* measurements of size and optical properties of single microparticles in an RF plasma," Phys. Plasmas **28**, 123701 (2021).

[49]F. Greiner, "Imaging Mie ellipsometry: Dynamics of nanodust clouds in an argon-acetylene plasma," Plasma Sources Sci. Technol. **21**, 065005 (2012).

[50]S. Groth, F. Greiner, B. Tadsen, and A. Piel, "Kinetic Mie ellipsometry to determine the time-resolved particle growth in nanodusty plasmas," J. Phys. D **48**, 465203 (2015).

[51]F. Greiner, A. Melzer, B. Tadsen, S. Groth, C. Killer, F. Kirchschlager, F. Wieben, I. Pilch, H. Krüger, D. Block, A. Piel, and S. Wolf, "Diagnostics and characterization of nanodust and nanodusty plasmas," Eur. Phys. J. D **72**, 81 (2018).

[52]N. Kohlmann, F. Wieben, O. Han Asnaz, D. Block, and F. Greiner, "High-precision in-situ size measurements of single microparticles in an RF plasma," Phys. Plasmas **26**, 53701 (2019).

[53]O. H. Asnaz, H. Jung, F. Greiner, and A. Piel, "Size and density evolution of a single microparticle embedded in a plasma," Phys. Plasmas **24**, 083701 (2017).

[54]L. P. T. Schepers, J. Beckers, and W. L. IJzerman, "Determination of microparticle characteristics in an etching plasma," Contrib. Plasma Phys. **58**, 985–994 (2018).

[55]S. H. Hong and J. Winter, "Size dependence of optical properties and internal structure of plasma grown carbonaceous nanoparticles studied by *in situ* Rayleigh-Mie scattering ellipsometry," J. Appl. Phys. **100**, 64303 (2006).

[56]S. Barbosa, F. R. Onofri, L. Couëdel, M. Wozniak, C. Montet, C. Pelcé, C. Arnas, L. Boufendi, E. Kovacevic, J. Berndt, and C. Grisolia, "An introduction to light extinction spectrometry as a diagnostic for dust particle characterisation in dusty plasmas," J. Plasma Phys. **82**, 615820403 (2016).

[57]S. Dap, D. Lacroix, R. Hugon, and J. Bougdira, "Retrieving particle size and density from extinction measurement in dusty plasma, Monte Carlo inversion and Ray-tracing comparison," J. Quant. Spectrosc. Radiat. Transfer **128**, 18–26 (2013).

[58]S. Yatom, J. Bak, A. Khrabryi, and Y. Raitses, "Detection of nanoparticles in carbon arc discharge with laser-induced incandescence," Carbon **117**, 154–162 (2017).

[59]K. J. Daun, B. J. Stagg, F. Liu, G. J. Smallwood, and D. R. Snelling, "Determining aerosol particle size distributions using time-resolved laser-induced incandescence," Appl. Phys. B **87**, 363–372 (2007).

[60]T. A. Sipkens, R. Mansmann, K. J. Daun, N. Petermann, J. T. Titantah, M. Karttunen, H. Wiggers, T. Dreier, and C. Schulz, "In situ nanoparticle size measurements of gas-borne silicon nanoparticles by time-resolved laser-induced incandescence," Appl. Phys. B **116**, 623–636 (2014).

[61]G. S. Eom, C. W. Park, Y. H. Shin, K. H. Chung, S. Park, W. Choe, and J. W. Hahn, "Size determination of nanoparticles in low-pressure plasma with laser-induced incandescence technique," Appl. Phys. Lett. **83**, 1261–1263 (2003).

[62]T. Donders, T. Staps, and J. Beckers, "Time-synchronized microwave cavity resonance spectroscopy and laser light extinction measurements as a diagnostic for dust particle size and dust density in a low-pressure radio-frequency driven nanodusty plasma," Appl. Sci. **12**, 12013 (2022).

[63]C. Cui and J. Goree, "Fluctuations of the charge on a dust grain in a plasma," IEEE Trans. Plasma Sci. **22**, 151 (1994).

[64]H. M. Mott-Smith and I. Langmuir, "The theory of collectors in gaseous discharges," Phys. Rev. **28**, 727 (1926).

[65]M. A. Lieberman and A. J. Lichtenberg, *Principles of Plasma Discharges and Materials Processing* (John Wiley & Sons, Inc., 2005).

[66]M. A. Van Ninhuijs, K. A. Daamen, J. G. Franssen, J. Conway, B. Platier, J. Beckers, and O. J. Luiten, "Microwave cavity resonance spectroscopy of ultracold plasmas," Phys. Rev. A **100**, 061801 (2019).

[67]J. Beckers, F. M. J. H. Van De Wetering, B. Platier, M. A. W. Van Ninhuijs, G. J. H. Brussaard, V. Y. Banine, and O. J. Luiten, "Mapping electron dynamics in highly transient EUV photon-induced plasmas: A novel diagnostic approach using multi-mode microwave cavity resonance spectroscopy," J. Phys. D **52**, 034004 (2018).

[68]B. Platier, T. J. A. Staps, M. Van Der Schans, W. L. Ijzerman, and J. Beckers, "Resonant microwaves probing the spatial afterglow of an RF plasma jet," Appl. Phys. Lett. **115**, 254103 (2019).

[69]J. C. Slater, "Microwave electronics," Rev. Mod. Phys. **18**, 441 (1946).

[70]M. A. Biondi, "Measurement of the electron density in ionized gases by microwave techniques," Rev. Sci. Instrum. **22**, 500–502 (1951).

[71]F. M. J. H. Van De Wetering, W. Oosterbeek, J. Beckers, S. Nijdam, E. Kovačević, and J. Berndt, "Laser-induced incandescence applied to dusty plasmas," J. Phys. D **49**, 295206 (2016).

[72]I. V. Schweigert, A. L. Alexandrov, and D. A. Ariskin, "Effect of nanoparticles on discharge plasma and first steps of their formation," Plasma Chem. Plasma Process. **34**, 671–702 (2014).

[73]U. V. Bhandarkar, M. T. Swihart, S. L. Girshick, and U. R. Kortshagen, "Modelling of silicon hydride clustering in a low-pressure silane plasma," J. Phys. D **33**, 2731 (2000).

[74]P. K. Shukla and A. Mamun, *Introduction to Dusty Plasma Physics* (IOP Publishing, 2002).

[75]M. Gatti and U. Kortshagen, "Analytical model of particle charging in plasmas over a wide range of collisionality," Phys. Rev. E **78**, 046402 (2008).

[76]B. Tadsen, F. Greiner, and A. Piel, "On the amplitude of dust-density waves in inhomogeneous dusty plasmas," Phys. Plasmas **24**, 033704 (2017).

05 September 2023 12:33:15